Neural correlates of radial frequency trajectory perception in the human brain

Diana J. Gorbet Centre for Vision Research, York University, Toronto, ON, Canada

Frances Wilkinson Centre for Vision Research, York University, Toronto, ON, Canada

Hugh R. Wilson Centre for Vision Research, York University, Toronto, ON, Canada

Radial frequency (RF) motion trajectories are visual stimuli that consist of a difference of Gaussians moving along a closed trajectory defined by a sinusoidal variation of the radius relative to a circular path. In the current study, multivoxel fMRI analyses demonstrated that spatial patterns of activity in visual regions V2, V3, and MT can predict RF motion trajectory shape regardless of whether an observer can behaviorally identify the shape or not. This result suggests that processing in these regions is concerned with local properties of the trajectories and not directly linked with a conscious percept of global trajectory shape. Whole-brain analyses show that RF motion trajectories also evoke premotor and posterior parietal cortical activity that may be a neural correlate of shape recognizability. Further, comparisons with activity evoked by static versions of the RF shapes reveal cue-invariant processing in regions of the posterior parietal and occipitotemporal cortices. Interestingly, the RF motion trajectories evoke patterns of dorsal visual stream cortical activity typical of visually guided movement preparation or action observation, suggesting that these stimuli may be processed as potential motor actions rather than as purely visual experiences.

Introduction

Periodic closed-circuit motion is an important component of many types of biological motion when viewed relative to body translation (Johansson, 1973; Johansson, 1976; Tsai, Shah, Keiter, & Kasparis, 1994). During rhythmic movements like walking, the motion trajectories of joints such as the knee are periodic since they begin and end in the same spatial location with respect to the rest of the body for each cycle of the movement. Similarly, cyclical closed-circuit motions of the arm and hand are often observed during the production of gestural, nonverbal communication (Ladewig, 2011; Xiong & Quek, 2006). Since closed-circuit visual motion forms an integral component of human biological motion, it stands to reason that perception of periodic motion might be involved in motor learning and our ability to understand the movements and intentions of other people.

In a previous study, we used fMRI to investigate the neural correlates of the perception of closed-circuit visual motion in early cortical visual areas, motion processing region MT, and regions of the superior temporal sulcus that are involved with processing biological movements (Gorbet, Wilkinson, & Wilson, 2012). Participants were presented with a dot moving along radial frequency (RF) motion trajectories that were based on deformations of a circular movement path (Or, Thabet, Wilkinson, & Wilson, 2011). RF patterns are formed by sinusoidally modulating the radius of a circular trajectory in polar coordinates (Wilkinson, Wilson, & Haback, 1998). The RF motion trajectories used in our previous study ranged from RF2 to RF5 and therefore formed familiar, identifiable shapes that were oval-, triangle-, diamond-, and star-like. Results of the study demonstrated that spatial patterns of BOLD fMRI activity in visual regions V2 and V3 predict the shape of these low-frequency, periodic radial frequency (RF) motion trajectories. A trend toward statistically significant decoding was also observed in MT. Further, V2 and V3 successfully decoded motion trajectories in spite of variation in the RF amplitudes and phases within individual blocks of shapes. These results provide convincing evidence that

Citation: Gorbet, D. J., Wilkinson, F., & Wilson, H. R. (2014). Neural correlates of radial frequency perception in the human brain. *Journal of Vision*, *14*(1):11, 1–19, http://www.journalofvision.org/content/14/1/11, doi:10.1167/14.1.11.

doi: 10.1167/14.1.11 Received July 17, 2013; published January 10, 2014 ISSN 1534-7362

these visual regions are involved in processing periodic visual motion. However, the findings of this initial study do not specifically address whether this processing is directly linked to the conscious perception of global trajectory shape from visual motion or to a lower level process such as the detection of local curvature (which necessarily varies for different RF motion trajectory shapes). Therefore, in the current study, we sought to examine whether decoding of RF motion trajectory shape by early visual regions is associated with detection of local properties of the trajectories or is instead directly linked to global shape perception.

We hypothesized that if a region is involved in the perception and conscious recognition of the overall shape of a motion trajectory, presenting an observer with indiscriminable trajectory shapes might eliminate the ability to predict shape from spatial patterns of fMRI voxel activity within V2 and V3. In contrast, if these regions are instead involved in processing local properties of motion trajectories or perhaps global properties that do not directly contribute to a conscious percept of shape, one would expect that activity within them will predict trajectory shape regardless of whether that shape is identifiable to an observer or not. We tested this hypothesis in the current study by comparing fMRI activity associated with observing RF visual motion trajectories that formed identifiable, low-frequency RF4 and RF5 shapes and behaviorally indiscriminable high-frequency RF9 and RF10 trajectories. In addition, we examined patterns of functional activity associated with the presentation of static versions of the RF shapes.

The main findings of this study demonstrate that visual regions V2, V3, and additionally, MT can decode different RF motion trajectory shapes regardless of whether the observer is able to discriminate the trajectories behaviorally or not. Therefore these areas do not directly contribute to our conscious recognition of shape from RF motion but likely process differences in local properties occurring between different RF motion trajectory shapes. Comparing brain activity evoked by RF motion trajectories with that evoked by static versions of these shapes revealed regions of overlapping patterns of activity within the posterior parietal cortex (PPC) and within the occipitotemporal cortex. This result suggests that these regions process shape information in a cue-invariant manner. In contrast to these regions that appear to integrate shape information regardless of which visual cue defines a shape (i.e., contrast or motion), other regions displayed cue-dependent patterns of activity. In particular, activity in the lateral occipital complex seems mainly associated with processing static versions of the RF shapes. In contrast, activity within dorsal stream premotor cortex regions appears to be linked to our conscious recognition of RF shapes but only for the RF motion trajectory stimuli. Together, the data presented here start to provide a picture of how the brain processes and recognizes the shape of periodic, closed circuit visual motion and static versions of these shapes.

Methods

Participants

Participants in the study consisted of six women and four men (mean age 26.8± *SEM* 2.04 years). All individuals had normal or corrected-to-normal vision and were right handed. The York University Research Ethics Board human participants subcommittee approved the protocol used in the experiment. The experimental protocol was in compliance with the Declaration of Helsinki. All participants provided informed written consent prior to data collection.

Radial frequency stimuli

Radial frequency (RF) motion trajectories consisted of a dot moving along a periodic trajectory centered about a fixation cross (Figure 1a). The motion path was produced by applying a sinusoidal temporal modulation to the radius of an otherwise circular trajectory such that the dot moved at angular speed v and the dot's polar location r at time t was defined as

$$r(vt) = r_0[1 + \mathrm{Asin}(\omega \mathrm{vt} + \phi)], \quad (1)$$

where r_0 is the mean radius, A is the radial modulation amplitude, ω is the radial frequency, and ϕ is the phase angle of the trajectory (Gorbet et al., 2012; Or et al., 2011). The movement of the dot traced a trajectory that always began from a point directly to the right of the fixation cross, moved in a clockwise direction around the cross, and then ended at the location from which it began. During the presentation of RF motion stimuli, participants only saw the dot moving (i.e., the actual shape of the RF trajectory itself was never displayed). The mean radius (r_0) was set to 2° of visual angle. Radial frequencies (ω) included in the study were 4, 5, 9, and 10 cycles. Amplitude (A) and phase angle (ϕ) were varied from trial to trial to prevent adaptation to the stimuli. The phase angle defines the orientation of the trajectory. Changing this value results in a rotation of the shape described by the motion trajectory but it does not alter the starting position of the dot on the screen. Amplitude defines the size of the sinusoidal deviation of the radius of the motion trajectory relative to that of a circular trajectory. Amplitude ranges used in the study were many times higher than mean

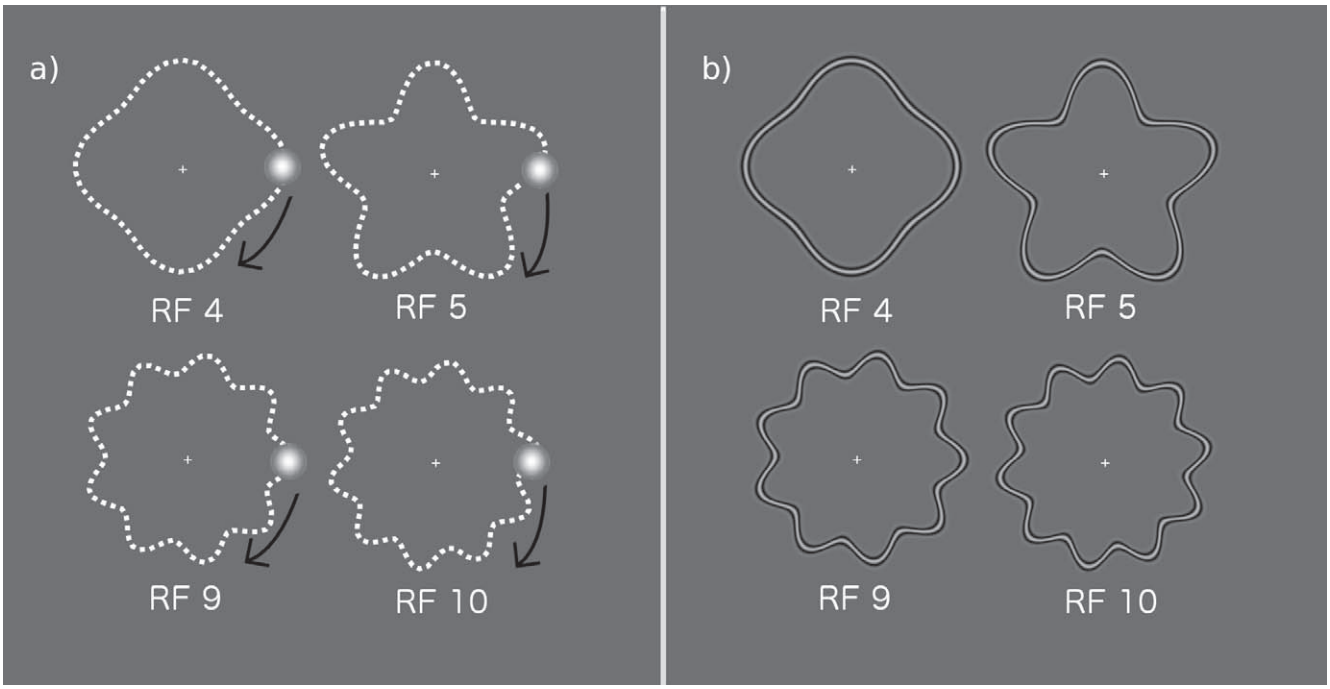

Figure 1. Schematic drawing of example radial frequency (RF) motion trajectories (a) and RF static images (b). In the motion stimuli, the dot traced a trajectory that always began from a location directly to the right of the fixation cross and then moved clockwise around the cross, ending at the location from which it started. Participants only saw the dot and the fixation cross (trajectory shape outlines were not visible during the experiment). The static RF stimuli were of identical shape, amplitude range, and retinotopic extent as the motion stimuli but lacked the motion component.

detection thresholds typically observed in individual participants (Or et al., 2011) ensuring that observers could readily detect the sinusoidal modulations.

The moving dot that traced the shape of trajectories consisted of a radially symmetric difference of Gaussians (DOG) defined as

$$\mathrm{DOG(R)} = 1.8\exp(-\mathrm{R}^2/\sigma^2) - 0.8\exp\left(-\mathrm{R}^2/(1.5\sigma)^2\right), \quad (2)$$

where R is the radius of the DOG and σ was set to 7.1 min of arc such that the peak spatial frequency was 2.74 c° and the bandwidth was 1.79 octaves at half amplitude. The contrast of the dot was 100% and the dot subtended a visual angle of approximately 0.6°.

Stimuli were equated so that ranges of properties including retinotopic extent, path length, and speed were extremely similar for the RF4 and RF5 trajectories and for the RF9 and RF10 trajectories (Table 1). The angular speed of the dot was also kept constant for all of the RF motion trajectories presented, such that the dot always took 3 s to complete one full cycle of rotation about the fixation cross. However, it is important to note that by keeping the angular speed constant, tangential speed (i.e., linear Cartesian speed) of the dot necessarily varied with the instantaneous radius as the dot's distance from the center changed along each trajectory. In other words, the tangential speed increased with the dot's distance from the central fixation point. Ranges of tangential speeds for each radial frequency are presented in Table 1. Curvature values necessarily differ when the frequency of an RF shape is changed. Ranges of curvatures for the shapes presented in this study are found in Table 2. Curvature is defined as

$$\mathrm{K} = (\mathrm{A}\omega^2 + \mathrm{A} + 1)/\left[r_0(1+\mathrm{A})^2\right], \quad (3)$$

RF	Minimum length (°)	Maximum length (°)	Minimum radius (°)	Maximum radius (°)	Minimum tangential speed (°/s)	Maximum tangential speed (°/s)
4	13.42	14.99	1.53	2.47	4.82	8.75
5	13.87	16.14	1.53	2.47	4.82	9.74
9	14.55	16.96	1.71	2.29	5.36	10.43
10	14.97	17.79	1.71	2.29	5.36	11.17

Table 1. Ranges of path lengths, radii, and speeds used for each RF motion trajectory.

RF	Minimum curvature ($^{\circ -1}$)	Maximum curvature ($^{\circ -1}$)
4	1.27	1.64
5	1.74	2.33
9	3.62	4.96
10	4.36	6.02

Table 2. Minimum and maximum curvature of the RF motion trajectory paths across the range of amplitudes tested.

where A = radial modulation amplitude, ω is the radial frequency, and r_0 is the mean radius of the RF trajectory.

Static versions of the RF motion trajectory stimuli described in the proceeding section were also generated such that they matched the ranges of amplitude, phases, mean retinotopic extent, and the spatial frequency bandwidth of the motion stimuli (Figure 1b).

Behavioral control experiment

Nine observers participated in a control experiment that was run to determine whether or not participants were able to reliably discriminate between high-frequency RF patterns matching the spatial and temporal characteristics of those presented during the fMRI portion of the experiment. The observers consisted of five women and four men (mean age 32.1 $\pm$ *SEM* 1.84 years). Of the nine observers, three also participated in the fMRI experiment.

The control experiment consisted of a two-alternative forced choice procedure. RF motion trajectories were tested separately from static RF images. Each trial contained two temporal intervals where each interval contained either an RF9 or an RF10 presented in random order. Each RF stimulus was presented for 3.0 s and the two intervals were separated by a 500 ms presentation of a visual noise mask to help prevent retinal afterimage contribution to stimulus discrimination. Participants were asked to report (with a button press) which interval contained the stimulus with the higher radial frequency. Phases and amplitudes of the stimuli were varied as they were in the MRI component of the study. Each participant performed four blocks of 30 trials each. Note that we did not psychophysically test discrimination of the low-frequency RF4 and RF5 shapes since the ability to reliably distinguish and identify these shapes has been previously demonstrated (Or et al., 2011).

MRI data collection and analysis

The stimuli used in the study were projected onto a screen that was viewed by participants via a mirror measuring 16 × 12 cm placed over the head coil. Participants' eyes were approximately 13 cm away from the mirror (depending on individual head size and position in the head coil). The resolution of images projected was 1280 × 1024 and the refresh rate of the projector was 60 Hz.

MRI data were collected using a 3T Siemens Magnetom Avanto MRI system with a 32-channel head coil at York University. T1-weighted anatomical images were collected using 192 slices in the sagittal orientation, TR = 1900 ms, TE = 2.44 ms, flip angle = 9°, FoV = 240 mm, and a voxel dimension of 0.9 × 0.9 × 1.0 mm. Functional images were collected using T2*-weighted, gradient echoplanar imaging with FoV = 192 mm, TR = 2500 ms, TE = 30 ms, and flip angle = 90°. Thirty nine 3.0 mm thick slices were collected with an interleaved acquisition, zero gap, and a voxel dimension of 2.0 × 2.0 × 3.0 mm. Using this protocol, we collected data from the entire cortex of all participants. However, these parameters only partially covered the cerebellum in most participants.

Localizer scans

Regions of interest were localized with independent localizer runs (described in detail below). In general, processing of all functional localizer data included motion correction using the volume temporally closest to the acquisition of the anatomical scan as the reference volume. Head movement did not exceed 1 mm in any direction for all runs used for localization. Slice time correction and linear trend removal were applied to each localizer run. In addition all data were spatially smoothed using a 4 mm full width half maximum isotropic kernel.

Retinotopic mapping of early visual areas

Retinotopic mapping was performed to define the borders between visual areas V1, V2, V3, V3A, and V4 (Engel, Glover, & Wandell, 1997; Sereno et al., 1995). The protocol used rotating contrast-reversing (8 Hz) checkerboard wedges with a polar angle of 45° spanning a visual angle of approximately 0.4° to 6° eccentricity. A small dot at central fixation changed colour randomly every 0.5–3.0 s. To aid participants in maintaining central fixation and attention, they were required to press a button each time the fixation dot turned red. Each full cycle of wedge rotation lasted 60 s while the wedge moved around the fixation dot to eight locations (remaining at each location for 7.5 s). The run consisted of eight full cycles of rotation proceeded and followed by initial and final fixation periods of 12.5 s giving a total run duration of 505 s.

Retinotopic maps were generated for each participant using cross-correlation analyses of BOLD signal phase lag in response to the stimulus (Slotnick & Yantis, 2003). Each cycle of the BOLD time series was segmented into eight phases corresponding to the eight different wedge locations. For each phase, a hemodynamic response model was cross-correlated with the time series of each voxel. Voxels that surpassed a correlation threshold of 0.20 were then assigned a color associated with the stimulus phase that resulted in maximal correlation. The resulting map was projected onto an inflated cortical surface representation of anatomical T1-weighted MRI data for each participant. Regions of interest were defined for each participant by identifying reversals in the phase of map coloration.

MT localizer

The MT localizer consisted of a single functional run that lasted 297.5 s. The run consisted of randomly alternating blocks of either coherently translating dots or static dots. In both cases, the direction of dot translation or the pattern of static dots changed every 2 to 5 s. Four blocks of each of the two conditions were presented. Each block was 17.5 s long and separated with a baseline fixation period of equal duration. Participants were instructed to fixate on a central cross for the entire run. Contrasting the BOLD responses associated with moving and stationary dots resulted in reliable bilateral localization of MT in all participants.

Biological motion processing regions localizer

Biological motion related areas in the superior temporal sulcus region were localized using a block design run where blocks contained either intact point-light animations or scrambled animations (Grossman & Blake, 2001; Grossman et al., 2000; Peelen & Wiggett, 2006). Both types of animations consisted of 12 white dots on a gray background. In the intact animations, dot placement corresponded with the region of the actor's head and limbs and portrayed the entire body performing simple movements such as walking, kicking, or jumping. In scrambled animation blocks, dot locations were kept within the same screen region as those comprising intact animations and the motion trajectory of each individual dot was kept intact, but the starting spatial location of each dot's movement was randomized. Each block was 32.5 s long and consisted of 15 animations lasting approximately 1.5 s (separated by brief blank intervals). Each run contained three of each of the two types of blocks and blocks were separated by fixation periods lasting 17.5 s. The entire run lasted for 317.5 s.

Experimental scans

During the experimental data collection session, participants performed two types of block design runs: runs containing RF motion trajectory stimuli and runs containing static RF patterns. Participants performed four repetitions of each type of run, meaning that a total of eight runs were collected. RF motion runs contained only RF motion stimuli. Each block contained only a single type of radial frequency; either RF4, RF5, RF9, or RF10. Each run contained three blocks of each frequency in a pseudorandom order. Within each block, a total of eight separate trajectories were shown and the amplitude and phase of each trajectory was varied to prevent participants from adapting to the stimulus. The time taken by the dot to trace a single RF motion trajectory was 3.0 s and trajectories were separated with 0.17 s blank fixation intervals. In static RF runs, each shape was also presented for 3.0 s with a 0.17 s interstimulus interval. Within each block, one of the eight stimuli presented was a circular motion trajectory in the case of RF motion runs or a static circle in the case of static RF runs instead of an RF shape. Participants were required to respond to the appearance of a circle by pressing a button to ensure that attention was being paid to the task.

Region of interest multivoxel pattern analysis

Preprocessing of each functional data run included motion correction using the volume closest to the time of anatomical scan acquisition as the reference volume. In addition, the head motion of each participant was viewed in six coordinates from the control room immediately after each functional run was collected to confirm that movement of the head did not exceed 1 mm in any direction. None of the participants were required to repeat any runs due to excess head movements in the scanner. Also, during preprocessing, visual inspection of the data, plots of head movement over time, and movies of head movement over time confirmed that all runs included in the final analyses did not contain head movements over 1 mm and that the data were free from scanner-related artifacts. Slice time correction and linear trend removal were applied to each functional run. The data were left in native subject space and spatial smoothing was not performed for the region of interest (ROI) analysis.

Multivoxel pattern analysis (MVPA) utilized a linear support vector machine (SVM) classification approach to test whether patterns of spatial voxel activity in regions of interest predicted RF shape (see Nichols & Holmes, 2001). RF motion trajectories and static RF images were tested separately. SVM tests of classification accuracy were performed separately for RF4

versus RF5 shapes and for RF9 versus RF10 shapes. Input into classification analyses consisted of t value response pattern estimates. In the analyses, BOLD signal values for each voxel were z normalized to remove differences in mean activation levels associated with different categories.

A leave-one-run-out cross-validation approach with 1,000 permutations was used within each region of interest to assess the statistical significance of decoding accuracy. For each participant, training data used to create the classifier's discriminant function consisted of three of the four runs collected (for either motion trajectory or static image data sets). The fourth run was then used as test data to evaluate the classifier's performance after training. This process was repeated until each run had been left out for testing once, resulting in a four-fold cross-validation of permutation testing in each region of interest for each participant. The mean accuracy of the classifier across the four folds (measured as percent correct classification) was used as the estimate of classifier performance for each participant. Statistical significance was defined as mean classification accuracy of the test data meeting or exceeding the 95th percentile of the distribution obtained from permutation testing. Chance level was 50% for each two-class comparison.

Whole-cortex recursive feature elimination multivoxel pattern analysis

Each participant's anatomical and functional data series were preprocessed as described in the region of interest multivoxel pattern analysis section above. In addition the data were Talairach normalized prior to running linear support vector machine (SVM) recursive feature elimination (RFE; see De Martino et al., 2008) for the purpose of group comparisons. The steps described below were followed separately for both the RF motion trajectory and RF static image data sets. Separate SVM RFE analyses were done in each participant for comparisons between discrimination of RF4 and RF5 and between RF9 and RF10.

Voxel intensity thresholding of anatomical T1 images was used to create segmentation masks of the cortex for each participant. These masks were generated utilizing the spatial resolution of T1 anatomical images (i.e., 0.9 $\times$ 0.9 $\times$ 1.0 mm) but were transformed to the spatial resolution of functional data sets (i.e., 2.0 $\times$ 2.0 $\times$ 3.0 mm) prior to RFE analysis. In brief, SVM RFE is a multivariate approach that allows for whole-brain detection of discriminative spatial patterns of voxel activation without a priori hypotheses regarding the anatomical location of discriminative voxels (see De Martino et al., 2008; Guyon, Weston, & Barnhill, 2002). The RFE technique uses a wrapper feature selection strategy with a linear support vector machine (SVM) classifier to find the subset of voxels which maximize generalization of the classifier. The process uses a stepwise voxel elimination approach such that weight magnitudes from SVM classifier results are used as the ranking criterion for voxel selection. With each iteration the voxels which are most sensitive for class discrimination are extracted and then the classifier is retrained using this more sensitive reduced set of voxels.

Prior to RFE computation, univariate activation-based voxel reduction was performed on each data set to select the top 33% of voxels demonstrating task-related activity for second-level analysis. This filtration technique reduced the number of voxels from approximately 40,000–50,000 to approximately 13,000–16,500 in each participant. Constraining the search space of the RFE algorithm has been shown to reduce the possibility of overfitting (Guyon, Weston, & Barnhill, 2002) and using univariate feature selection as a constraint method has been demonstrated to provide more robust results than performing SVM RFE without univariate feature selection (De Martino et al., 2008). The final desired percentage of "surviving" voxels was specified as 8% of this filtered data set, leaving a final population of around 1,000 voxels in each participant.

Within BrainVoyager, the SVM RFE process utilizes two nested levels of cross-validation. The first level of cross-validation was set to five folds. SVM weighting values for the final set of surviving voxels were derived from the mean results of these folds. Within each fold of this first level of cross-validation, second-level cross-validation was performed such that the trials were partitioned into 50 different "splits" for each of 10 gradual voxel elimination steps. The final set of surviving voxels for each reduction level were obtained by selecting the voxels with the highest mean absolute weights across all splits. Ranking scores were spatially smoothed prior to selection of voxels using a full width at half maximum filter of 1.5 mm. Smoothing the scores in this manor favors the selection of clusters of voxels with significant SVM weight rankings rather than isolated voxels which could more easily achieve high weightings by chance alone. This process resulted in the generation of two separate SVM weight maps for each participant's RF motion trajectory data and two weight maps for each participant's static RF image data. The absolute value of a weight ranking directly reflects the importance of that voxel in discriminating the two classes being examined.

MVPA approaches are generally performed in native subject anatomical space (rather than on data which has been transformed to a normalized anatomical space). Therefore, to help validate our approach, we visually compared the spatial locations of Tailarach normalized MT regions defined from independent

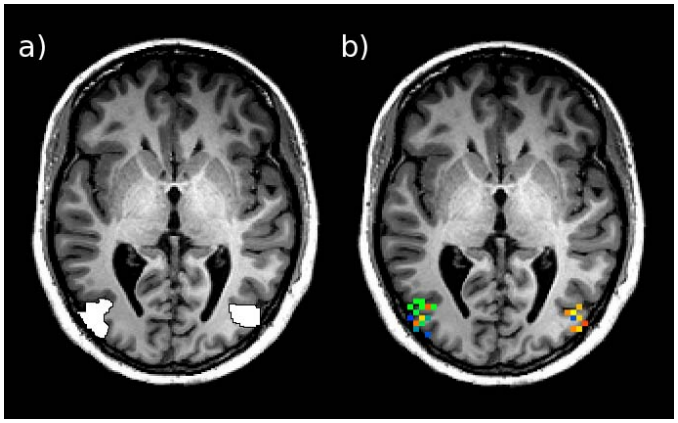

Figure 2. Visual validation of the prerecursive feature elimination Talairach normalization procedure. An example Talairach normalized brain slice ($z = 2$) collected from a single participant demonstrating the correspondence between MT regions detected using (a) a localizer scan and (b) the voxels chosen by the RFE analysis of RF4 versus RF5 motion trajectory discrimination. The proportion of overlapping voxels were not quantified but data were visually inspected to confirm approximate colocalization.

localizers in each participant, with the spatial locations of voxels chosen as significant by RFE analysis in and around the typical anatomical location of MT in individual RF motion trajectory data sets. We chose region MT for this validation of our methodology because it was easily and robustly localized in all participants and because it significantly decoded RF motion trajectory shape in the ROI multivoxel analyses in most participants. In all cases, significant voxels chosen by the RFE MVPA approach had an excellent correspondence with the region determined by localization (for example, see Figure 2) giving us confidence that the anatomical normalization of the data did not compromise the whole-brain MVPA.

To quantitatively compare the extent to which cortical regions are involved in discrimination of low frequency compared with high-frequency RF shapes, RF4/RF5 discrimination and RF9/RF10 discrimination weight maps were separated into two groups and a paired t test was performed comparing the absolute SVM weightings at each included voxel in the two conditions. A conservative cluster-based threshold of 10 consecutive voxels was used. Test results were then visualized on an inflated Talairach normalized brain.

Group general linear model region of interest comparison of high- and low-frequency RF shapes

A region of interest general linear model analysis was used to compare levels of BOLD activity associated with the low-frequency versus high-frequency conditions (separately for the RF motion and RF static data sets). Preprocessing of the data included motion correction (as described above), slice time correction, and linear trend removal. The data were ACPC aligned (i.e., rotated about the anterior commisure–posterior commisure plane) but left in native subject space. No spatial smoothing was used in this analysis. Design matrices for the general linear model (GLM) consisted of each participant's stimulation protocol convolved with a hemodynamic response function. The low-frequency RF4 and RF5 conditions were grouped as a single predictor ("low frequency"). Similarly, the high-frequency RF9 and RF10 conditions were grouped as a single predictor ("high frequency"). Holm-Bonferroni corrected two-tailed independent t tests were used to test for statistically significant differences within each region of interest for the low- versus high-frequency conditions.

Group general linear model comparisons

Preprocessing of the data for whole-brain general linear model (GLM) analyses was performed as above for the whole-cortex multivoxel pattern analysis except that spatial smoothing of 4 mm was added. GLM design matrices consisted of each participant's stimulation protocol convolved with a hemodynamic response function. Blocks of data collected for RF4 and RF5 conditions were grouped as a single predictor (low frequency) and blocks of RF9 and RF10 stimuli were grouped as a second single predictor (high frequency). BOLD signal amplitude comparisons (contrasts) were made between the low-frequency and high-frequency conditions in RF motion and RF static data separately using two-tailed independent t tests. Conjunction analyses were also performed separately within the motion and static image data sets to test for voxels showing common activation in the low- and high-frequency conditions. A conjunction analysis was also performed on combined motion and static data to localize voxels that were active in both of the two data sets. Correction for multiple comparisons employed a false discovery rate (FDR) approach with q set to 0.01 along with cluster-based thresholding using 20 consecutive voxels.

Results

Behavioral data

The results of the behavioral control experiment are presented in Figure 3. The group mean percentage of correct responses for distinguishing the high-frequency RF motion trajectories was 57% ± standard deviation of 12.1%. Therefore the ability of observers to

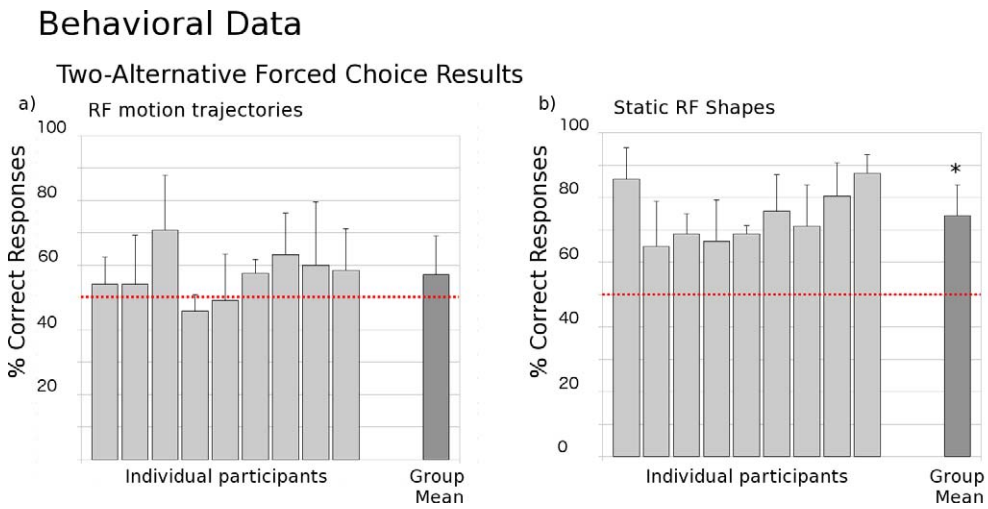

Figure 3. Behavioral results for discrimination of (a) high-frequency RF motion trajectories and (b) high-frequency static RF images. * indicates a significant difference from chance levels, $p < 0.0001$. Error bars represent standard deviation. The dashed horizontal line indicates the chance decoding level.

distinguish between RF9 and RF10 motion trajectories with the spatial and temporal properties of those presented in the fMRI portion of the study did not significantly differ from the chance level of 50% ($t = 1.74$, $p = 0.120$). In contrast, the group mean percentage of correct responses for distinguishing the high-frequency static RF images was 74.4% ± standard deviation of 9.5%. This value significantly differed from the expected chance value of 50% ($t = 7.70$, $p < 0.0001$). Therefore, in the fMRI study, observers may have been able to behaviorally distinguish the high-frequency static versions of the stimuli, although they were not explicitly asked to do so for the task.

fMRI task proficiency

All participants reported the presence of circular shapes (static or motion trajectories) in each block of each run with perfect or near perfect accuracy.

Region of interest multivoxel pattern analyses (MVPA)

Linear SVM MVPA classification tests were performed in regions of interest V1, V2, V3, V3A, V4, MT, and STS biological processing-related areas for discrimination of RF4 versus RF5 motion trajectories and separately for discrimination of RF9 versus RF10 motion trajectories. Group mean classification accuracies of the tested data met or exceeded the 95th percentile of distributions obtained from permutation testing within visual regions V2, V3, and MT on both sides of the brain and for both comparisons, with the exception of the RF9 versus RF10 comparison result which was just below significance in the right MT region. In other words, spatial patterns of BOLD activity within these regions successfully distinguished between RF4 and RF5 low-frequency trajectories and also between RF9 and RF10 high-frequency trajectories above the chance level of 50% (Figure 4a).

The same comparisons were also made in the static RF image data set; however, classification accuracy did not reach significance in any of the ROIs for either discrimination of RF4 versus RF5 shapes or RF9 versus RF10 shapes (Figure 4b).

Region of interest GLM analysis

ROI GLM analyses for RF motion stimuli revealed significantly greater activity in left V1, left V4, and bilaterally in MT for the low-frequency (RF4/RF5) trajectories compared with the high-frequency (RF9/RF10) trajectories. Activity associated with the high-frequency motion trajectories was not significantly greater than that associated with low-frequency trajectories in any of the regions (Table 3).

ROI GLM analyses for the static RF image data revealed significantly greater activity bilaterally in MT for the low-frequency condition. Right V1 had a significantly higher BOLD amplitude associated with the high-frequency stimuli (Table 3).

Whole-brain recursive feature elimination multivoxel pattern analysis

For the comparison between RF4/5 versus RF9/10 SVM weight maps for the motion trajectory data set, significantly higher weights (qFDR corrected $p < 0.05$)

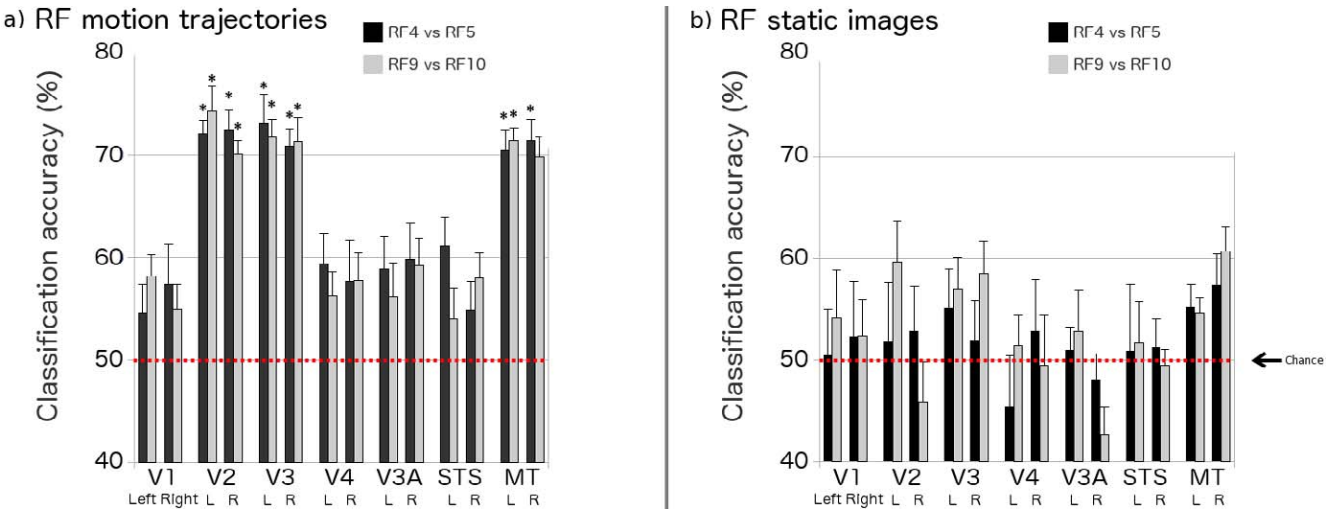

Figure 4. Group mean linear support vector machine classifier accuracies for discrimination between low-frequency shapes (black) and between high-frequency shapes (gray). Significance (*) was defined as a mean classification accuracy of the tested data meeting or exceeding the 95th percentile of the distribution from permutation testing. (a) RF motion data and (b) RF static data.

were found for the RF4/5 group of maps compared with the RF9/10 group of maps in the right premotor cortex, Brodmann Area 6 (centered on Talairach coordinates $x = 33$, $y = -1$, $z = 57$ and $x = 47$, $y = 2$, $z = 41$), the right inferior frontal gyrus, Brodmann Area 9 ($x = 46$, $y = 0$, $z = 20$) and bilaterally in the inferior parietal lobule, Brodmann Area 40 (centered on Talairach coordinates $x = 40$, $y = -50$, $z = 38$ and $x = -50$, $y = -48$, $z = 38$). No regions were detected in which group mean SVM weights were significantly higher in the RF9/10 maps (Figure 5a).

Region of interest	RF motion 4/5 > 9/10 (*t* value, corrected *p* value)	RF static 4/5 > 9/10 (*t* value, corrected *p* value)
Left V1	**2.25, 0.05**	−0.40, > 0.99
Right V1	0.78, > 0.99	**−3.99, 0.00078**
Left V2	2.68, 0.074	−1.90, 0.58
Right V2	2.74, 0.069	−1.19, > 0.99
Left V3	2.66, 0.071	−2.24, 0.28
Right V3	0.90, > 0.99	−1.06, > 0.99
Left V4	**3.76, 0.0022**	−0.77, > 0.99
Right V4	−0.45, 0.65	−1.05, > 0.99
Left V3A	0.71, 0.95	−0.18, 0.86
Right V3A	0.90, > 0.99	−0.88, > 0.99
Left MT	**4.86, 0.000014**	**5.91, 0.000014**
Right MT	**3.70, 0.0026**	**7.56, 0.000013**
Left STS	1.67, 0.67	0.88, > 0.99
Right STS	1.24, > 0.99	−1.04, > 0.99

Table 3. Results of Holm-Bonferroni corrected *t* test comparisons of BOLD activity associated with low- versus high-frequency shapes for the RF motion and RF static conditions separately. Adjusted *p* values are shown. Significant effects are shown in boldface.

A similar comparison between RF4/5 and RF9/10 SVM weight maps for the static RF image data revealed significantly higher weights (qFDR corrected $p < 0.05$) for the RF4/5 condition compared with the RF9/10 condition in the right inferior occipital gyrus, Brodmann Area 19 (centered on Talairach coordinates $x = 43$, $y = -74$, $z = -3$) and in the right inferior parietal lobule, Brodmann Area 40 (centered on Talairach coordinates $x = 48$, $y = -58$, $z = 36$). No regions were detected in which group mean SVM weights were significantly higher in the RF9/10 maps (Figure 5b).

Whole-brain general linear model analyses

Figure 6 shows the results of GLM comparisons on whole-brain data for both RF motion trajectory data and static RF image data. Conjunction analysis results show regions that are more active relative to baseline in both the low-frequency and high-frequency conditions (separately for motion and static data sets). In other words, these are regions that are involved in processing the stimuli regardless of radial frequency (Table 4 for RF motion data and Table 5 for static RF data). The results of contrasting BOLD activity associated with low-frequency shapes versus high-frequency shapes are found in Table 6 (RF motion stimuli) and Table 7 (static RF stimuli).

Group general linear model conjunction analysis results of RF motion and RF static data

Common regions found to be more active for low-frequency relative to high-frequency conditions in both

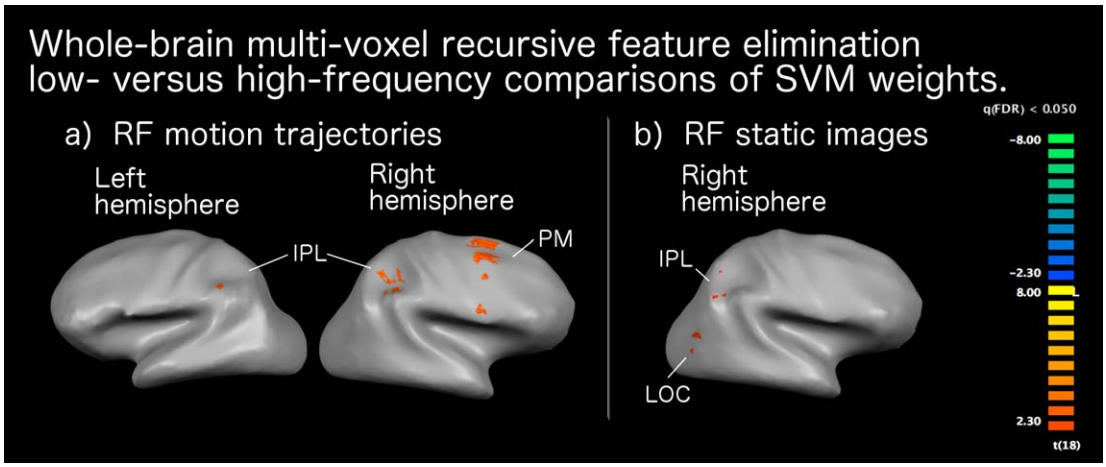

Figure 5. Regions where SVM weights obtained from recursive feature elimination were significantly higher in the low-frequency shape condition relative to the high-frequency shape condition in (a) the RF motion trajectory data and (b) the RF static image data.

the RF motion and RF static conditions included bilateral areas of the inferior parietal lobule and bilateral regions of the occipital-temporal cortices (Table 8 and Figure 7).

Discussion

Our previous work demonstrated that spatial patterns of BOLD fMRI activity within visual areas V2 and V3 are predictive of the shape of RF motion trajectories with frequencies ranging from RF2 to RF5 (Gorbet et al., 2012). Area MT also displayed a clear trend toward statistically significant decoding of trajectory shape, although that trend did not quite reach the level of statistical significance. The ability of multivoxel analyses to predict RF motion trajectory shape in these regions is independent of the phase and amplitude of trajectories therefore presenting the possibility that these regions are decoding the global shape of motion trajectories and directly contributing to our recognition of shape from the motion trajectories. Alternatively, these regions could be processing lower level characteristics of the stimuli such as curvature, which also varies with the overall shape. Therefore, the current study was designed to disentangle these possibilities by testing whether patterns of spatial activity in these regions (and others throughout the brain) can decode high-frequency RF motion trajectories that participants are unable to distinguish from one another behaviorally. If a region is directly involved in forming a conscious recognition of global trajectory shape, the presentation of behaviorally indiscriminable trajectories might abolish the ability to decode trajectory shape from spatial patterns of voxel activity within that region. In contrast, if a region is instead involved in processing local properties of motion such as trajectory curvature, it should decode high-frequency trajectory shapes regardless of an observer's inability to consciously distinguish between the shapes being viewed. In addition, this study looked at brain activity associated with static versions of the RF shapes observed in the RF motion portion of the experiment. Our main findings were as follows. First, spatial patterns of voxel activity within visual regions V2, V3, and MT are predictive of the shape of RF motion trajectories regardless of whether or not these trajectories are distinguishable to the observer. Second, whole-brain general linear model and recursive feature elimination analyses both suggest that conscious recognition of trajectory shape for the RF motion stimuli includes premotor and posterior parietal cortical (PPC) regions. Third, none of the localized regions of interest examined in this study revealed patterns of voxel activity that were predictive of the shape of static RF images; however, whole-brain analyses suggest that the PPC and the lateral occipital complex (LOC) play a role in this process when the stimulus lacks a motion component. Fourth, the data suggest that regions of the PPC and LOC contain visual cue-invariant brain areas involved in shape perception. The main findings from the whole-brain comparisons are summarized in Figure 8, below. In the sections that follow, we discuss these findings in detail.

Decoding of both low- and high-frequency RF motion trajectories in V2, V3, and MT

As in our previous study (Gorbet et al., 2012), the current study demonstrates that spatial patterns of BOLD activity in visual areas V2 and V3 can distinguish between RF4 and RF5 motion trajectories. In addition to these regions, MT was also found to be

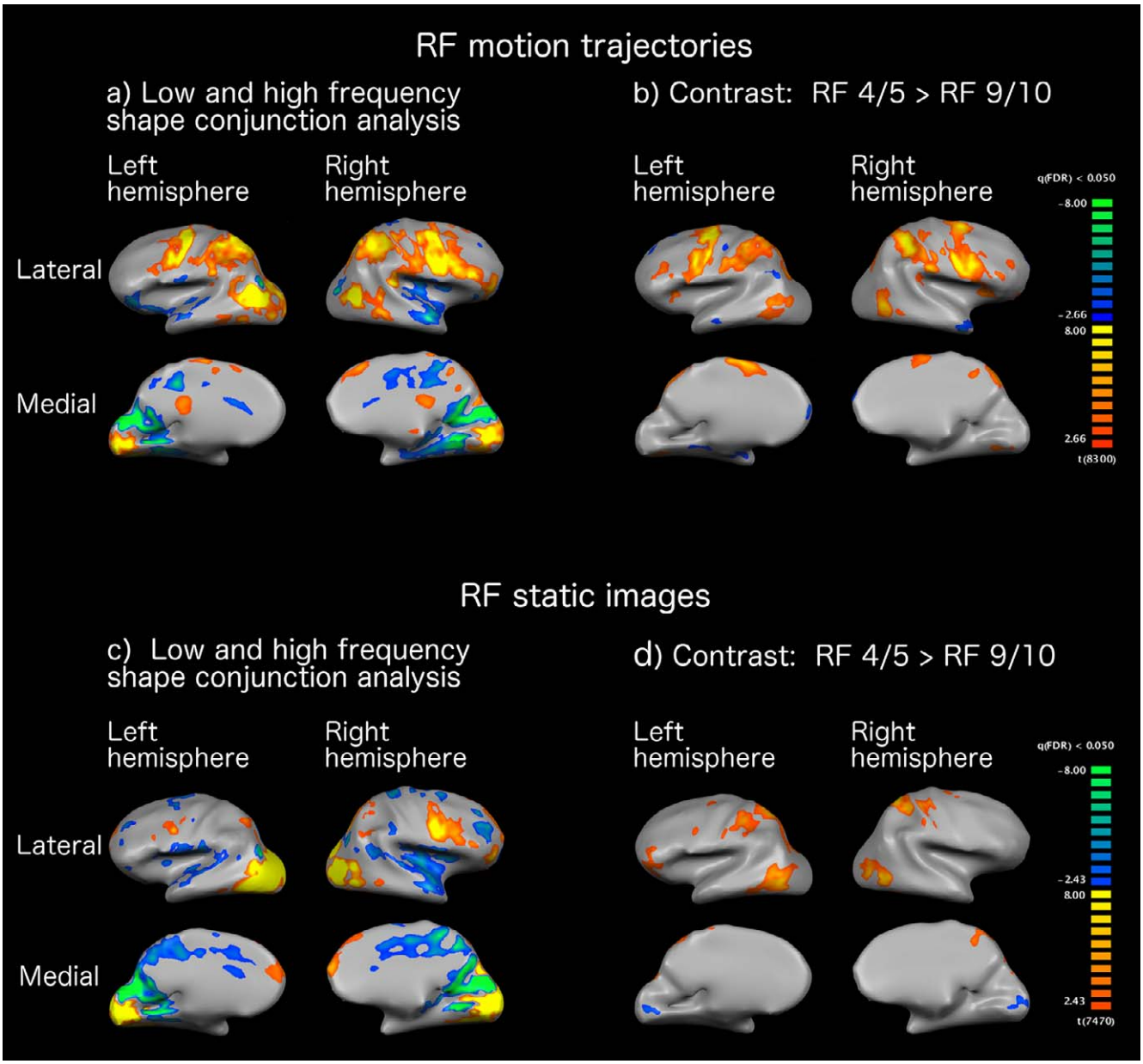

Figure 6. Group results from general linear model comparisons of fMRI activity. False color plots of significant *t* values are shown overlaid on an inflated normalized rendering of the brain of a single participant. (a) RF motion trajectories—conjunction analysis results showing common activity to both low-frequency (RF4/5) and high-frequency (RF9/10) trajectories, (b) RF motion trajectories—results of contrasts between BOLD activity associated with low- versus high-frequency trajectories. (c) Static RF images—conjunction analysis for low- and high-frequency static images, (d) Static RF images—results of contrast between low- and high-frequency conditions. Red-yellow colors indicate greater activity associated with low-frequency trajectories than with high-frequency trajectories. Blue-green colors demonstrate greater activity in the high-frequency conditions.

predictive of these trajectories in the current study. A trend toward statistical significance in MT was noted in the first study. However, in addition to decoding blocks of diamond-like RF4 and star-like RF5 motion trajectories, spatial patterns of voxel activity in V2, V3, and MT also distinguished between blocks of RF9 and RF10 trajectories. Although behavioral measures of discrimination were not collected during the MRI portion of the experiment, given the results of the behavioral control study conducted outside the magnet (see Figure 3), it is highly unlikely that participants were able to distinguish between the RF9 and RF10 motion trajectories. Therefore, we are confident that our finding that spatial patterns of BOLD activity in V2, V3, and MT can distinguish between RF9 and RF10 motion trajectories does not reflect a conscious percept of differences between the shapes of these trajectories. Rather, this finding suggests that decoding

Talairach coordinates of peak (*x*, *y*, *z*)	Details (Brodmann area of peak of activity)	Max. *t* value	# of voxels
−43, −7, 43	Left ventral premotor area (BA6) extending into dorsal and medial premotor regions	18.6	14,688
42, 3, 38	Right ventral premotor area (BA6) extending into dorsal and medial premotor regions	14.3	18,857
−32, −54, 45	Left inferior parietal lobule (BA 40) extending into superior parietal lobule	14.3	15,116
35, −50, 43	Right inferior parietal lobule (BA 40) extending into superior parietal lobule	11.2	16,611
−43, −67, 2	Left middle occipital gyrus (BA 37) extending into middle temporal gyrus	31.3	12,683
41, −60, 4	Right middle temporal gyrus (BA 37) extending into occipital lobe	31.5	9,001
−17, −87, −6	Left lingual gyrus (BA 18) extending posteriorly into occipital cortex	14.2	15,870
13, −85, −8	Right lingual gyrus (BA 18) extending posteriorly into occipital cortex	14.9	10,029
−49, −36, 22	Left insula (BA 13) extending into superior temporal sulcus	10.2	3,152
54, −35, 16	Right insula (BA 13) extending into superior temporal sulcus	13.2	3,988
30, 48, 9	Right middle frontal gyrus (BA 10)	9.4	5,124

Table 4. RF motion trajectories: Regions showing significant activity over baseline in a conjunction analysis of activity associated with both low- and high-frequency trajectories.

Talairach coordinates of peak (*x*, *y*, *z*)	Details (Brodmann area of peak of activity)	Max. *t* value	# of voxels
−16, 48, 22	Left superior frontal gyrus (BA 9 and 10)	9.6	11,022
19, 47, 23	Right superior frontal gyrus (BA9 and 10)	6.8	6,634
−46, −3, 36	Left ventral premotor area (BA 6)	8.7	2,644
43, 4, 34	Right ventral premotor area (BA 6)	11.6	11,831
−29, −67, 38	Left precuneus (BA 7)	6.7	2,442
24, −64, 39	Right precuneus (BA 7)	14.2	6,878
−26, −80, −8	Middle occipital gyrus (BA 18) extending toward occipital pole	33.6	38,138
25, −78, −5	Lingual gyrus (BA 18) extending toward occipital pole	41.4	42,904

Table 5. Static RF images: Regions showing significant activity over baseline in a conjunction analysis of activity associated with both low- and high-frequency images.

Talairach coordinates of peak (*x*, *y*, *z*)	Details (Brodmann area of peak of activity)	Max. *t* value	# of voxels
−42, −5, 41	Left ventral premotor area (BA 6) extending into dorsal and medial premotor regions	12.9	16,433
40, −1, 40	Right ventral premotor area (BA 6) extending into dorsal and medial premotor regions	11.5	18,037
−35, −48, 42	Left inferior parietal lobule (BA 40) extending into superior parietal lobule	8.5	22,588
34, −46, 42	Right inferior parietal lobule (BA 40) extending into superior parietal lobule	10	27,419
−44, −60, −5	Left middle occipital gyrus (BA 37) extending into middle temporal gyrus	6.2	3,775
45, −58, −5	Right middle temporal gyrus (BA 19) extending into middle occipital gyrus	7.8	6,786

Table 6. RF motion trajectories: regions showing significantly greater activity in low-frequency condition relative to high-frequency condition.

of trajectory shape in these early visual regions likely depends on the detection of local properties of the motion trajectories. Disentangling which specific local properties this process relies on is not possible from the data provided by the study presented here; however, some candidates are more likely than others. The mean radius and ranges of path lengths of the radial frequencies tested differed very little between the trajectories that were compared meaning that classification likely did not rely upon differences in the retinotopic extent of the stimuli (Table 1). On the other hand, ranges of curvatures necessarily differed between radial frequencies (Table 2), making curvature a potential local property being detected in regions that distinguish between trajectories. Also, keeping the angular speed constant for all of the RF motion trajectories unavoidably meant that the instantaneous tangential speed varied within each trajectory depending on the distance between the dot and the central fixation point. Previous work from our lab demonstrated that detection thresholds for RF motion trajectories do not significantly differ depending on whether angular speed or tangential speed are held constant (Or et al., 2011). However, it is possible that

Talairach coordinates of peak (*x*, *y*, *z*)	Details (Brodmann area of peak of activity)	Max. *t* value	# of voxels
−31, −57,40	Left superior parietal lobule (BA 7) extending medially and laterally	7.4	20,222
32, −44, 50	Right precuneus (BA 7) extending laterally	10.3	18,964
−23, −77, 27	Left precuneus (BA 31) extending into cuneus (BA 19)	6.8	8,435
17, −79, 31	Right precuneus (BA 31) extending into cuneus (BA 19)	5.5	2,091
−45, −65, −7	Left middle occipital gyrus (BA 37) extending into middle temporal gyrus and lateral occipital cortex	8.9	11,575
42, −64, −7	Right fusiform gyrus (BA 19) extending into middle temporal occipital and middle temporal cortex	7.8	13,611
−41, 41, 5	Left inferior frontal gyrus (BA 46)	6.1	8,522

Table 7. Static RF images: Regions showing significantly greater activity in low-frequency condition relative to high-frequency condition.

Talairach coordinates of peak (*x*, *y*, *z*)	Details (Brodmann area of peak of activity)	Max. *t* value	# of voxels
−35, −48, 44	Left inferior parietal lobule (BA 40) extending into superior parietal lobule	6.8	14,333
34, −43, 47	Right inferior parietal lobule (BA 40) extending into superior parietal lobule	7.8	12,843
−45, −66, −7	Left middle occipital gyrus (BA 37)	7.6	5,116
44, −60, −7	Right fusiform gyrus (BA 37)	5.8	3,914

Table 8. Conjunction analysis results demonstrating regions showing significantly greater activity in low-frequency condition relative to high-frequency condition in both the RF motion and RF static conditions.

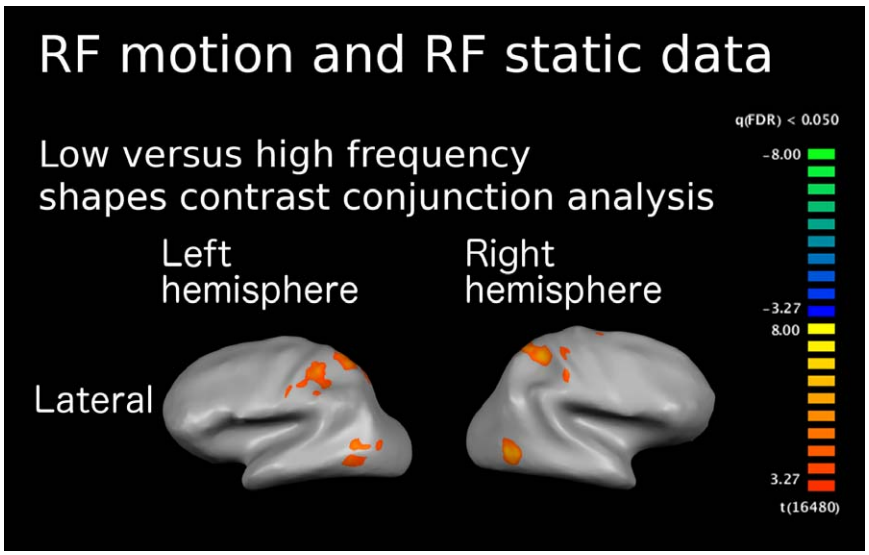

Figure 7. Conjunction analysis results demonstrating regions which are more active in response to low-frequency shapes relative to high-frequency shapes in both the RF motion and the static RF image conditions.

brain regions in which decoding occurred detected these changes in speed even if this detection does not directly contribute to behavioral discrimination of RF motion trajectories. Also, it is possible that the moving dot may have produced "motion streaks" (Geisler, 1999) as a result of temporal integration within the visual system. If present, these streaks could have provided local orientation and curvature cues that may have driven decoding. Finally, although participants were trained to fixate on the central fixation cross during presentation of the RF motion trajectories, eye movements were not monitored during the fMRI data collection. Therefore, we cannot rule out a potential contribution of eye movement-related processing to the successful decoding of trajectory shape in these regions. All of these possibilities present interesting opportunities for further examination of how V2, V3, and MT contribute to percepts of form from motion.

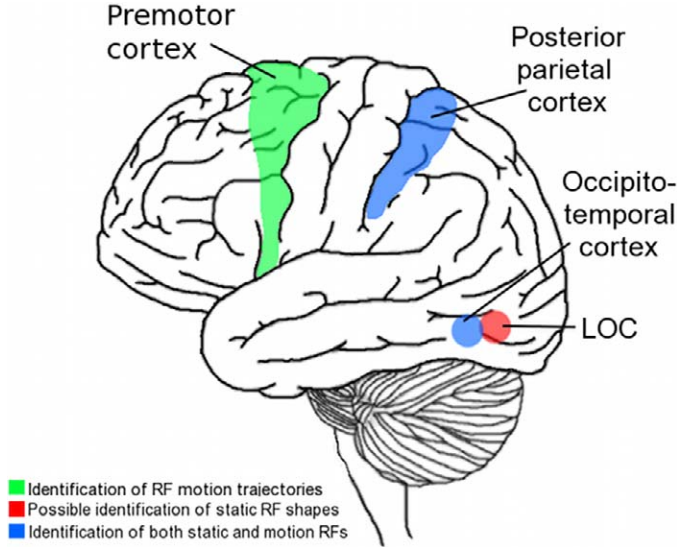

Figure 8. A summary of all of the whole-brain comparisons. Taken together, the findings suggest that processing and recognition of RF shapes utilizes (1) cortical activity specific for processing RF motion trajectories (shown in green), (2) putative cortical activity specific for processing static RF shapes (shown in red), and (3) cue-invariant cortical activity involved in processing RF shapes defined by either motion or contrast (shown in blue).

The absence of significant decoding in V4, which is known to play a role in shape perception (see Pasupathy, 2006), is puzzling. However, it is important to point out that a lack of statistically significant multivoxel classification in a region does not rule out the possibility of a role in processing RF shape information. MVPA depends on a topographical organization of neural responses within a tested region. A region in which no significant decoding can be detected could simply contain a spatial organization of neural responses that is not compatible with this approach. Therefore, our data do not shed light on any potential role of V4 in this processing but neither does it rule out a potential role for this region.

Similarly, the absence of significant shape decoding in the superior temporal sulcus regions isolated with our biological motion localizer could simply signify that this area does not contain the requisite spatial organization of neuronal responses needed for detection with a multivoxel approach. Alternatively, it is also possible that this region is not involved in processing local components of biological motion (for example, the periodic motion seen at a single joint during a rhythmic or repetitive motion) and is instead involved with processing whole-body motion. Indeed, the way in which this region was localized suggests a closer association with whole-body biological motion processing since it was more active for intact point-light stimuli than it was for scrambled stimuli containing the same components at random starting locations. The scrambled stimuli, like the individual RF motion trajectories, lack the coordinated shape and pattern of movement associated with true biological motion, providing a potential explanation for why the latter cannot be decoded in the posterior STS region. Also, unlike true biological motion which consists of local periodic motion around multiple points simultaneously, the RF motion trajectories only rotate about a single fixation point, providing another possible reason for a lack of decoding in the STS.

In contrast to the findings for the RF motion data, region of interest multivoxel analyses for the static RF image condition did not yield any significant results in any of the regions tested using a permutation test approach. This null result is surprising given how consistently MVPA of the motion data revealed significant decoding in V2, V3, and MT. However, permutation testing is a highly conservative approach that requires very high classification accuracies relative to presumed chance levels before a result may be considered significant. A less conservative one-sample t test versus an assumed chance level of 50% successful decoding does reveal significant differences in left V2 and left V3 for the static RF9 versus static RF10 comparison of classifier results (V2: $t = 2.50$, $p < 0.05$; V3: $t = 2.49$, $p < 0.05$), and in left and right MT for both the RF4 versus RF5 comparisons (left MT: $t = 2.68$, $p < 0.05$; right MT: $t = 2.84$, $p < 0.05$) and the RF9 versus RF10 comparisons (left MT: $t = 3.42$, $p < 0.01$; right MT: $t = 3.85$, $p < 0.005$). One-sample t tests do not reveal significant differences in decoding versus chance for any of the other regions of interest. However, these potentially significant decoding results in V2, V3, and MT for the static stimuli are not nearly as consistent as the permutation results for the RF motion trajectory data. It is possible that the nonsignificant permutation tests for the static stimuli could be related to neuronal adaptation given that each static image was presented for 3.0 s. Adaptation would have resulted in overall less signal strength in each block of static stimuli. This possibility could be tested with static RF patterns presented more rapidly. Alternatively, differential contribution of the magnocellular and parvocellular visual pathways in the moving versus static stimuli could be a relevant factor in our null finding for the static shapes.

Identification of RF motion trajectories in the mirror neuron system?

Along with region of interest multivoxel analyses, we also examined whole-brain data using general linear model and multivoxel approaches. We found that both low-frequency (i.e., RF4 and RF5) and high-frequency

(i.e., RF9 and RF10) motion trajectories evoke bilateral BOLD fMRI activity in the dorsal and ventral premotor cortices, medial premotor cortex, superior and inferior parietal lobules, primary somatosensory cortex, middle and inferior temporal, and a large portion of the occipital cortex (see Figure 6a and Table 4). However, activity in premotor (dorsal, ventral, and medial), posterior parietal (superior and inferior), and temporal cortex (middle and inferior) was significantly higher in response to the low-frequency motion stimuli relative to the high-frequency stimuli (Figure 6b and Table 6). In addition, multivoxel recursive feature elimination (RFE) demonstrated that SVM weights are significantly higher for the low-frequency stimuli relative to the high-frequency stimuli bilaterally in the inferior parietal lobules (IPL) and in right hemisphere dorsal and ventral premotor cortex (Figure 7). The larger the absolute value of an SVM weight, the more sensitive that particular voxel is for a class discrimination (see De Martino et al., 2008). Therefore, this result reveals that these premotor and inferior parietal regions are more highly involved in decoding the recognizable low-frequency trajectories than the behaviorally indiscriminable high-frequency trajectories. Taken together with the finding of greater BOLD signal in response to low-frequency stimuli in these regions, this result suggests that activity in premotor cortex and the inferior parietal lobule could be a neural correlate of the degree of global shape processing and/or the conscious identification of the shape of an RF visual motion trajectory.

The premotor-parietal regions activated by the RF motion trajectories are integral in performing the visual-to-motor transformations required for producing voluntary movements in response to visual stimuli. These highly interconnected regions integrate sensory information to form an internal model of the spatial locations of objects in the environment relative to each other and relative to the body itself (see Rizzolatti & Matelli, 2003). This integrated sensory information is then transformed by this neural circuitry into a motor plan that can be used to guide the body to an object of interest (see Battaglia-Mayer, Caminiti, Lacquaniti, & Zago, 2003). However, in addition to being crucial for the preparation of sensory-guided movements, these dorsal stream visual-motor regions (especially the ventral premotor cortex and the inferior parietal lobule) also comprise the action execution—action observation or "mirror neuron system" (see Rizzolatti & Sinigaglia, 2010). The mirror neuron system (MNS) allows an observer to obtain a first-person understanding of the motor intentions of other people. The task performed in this study required passive observation of RF shapes with the only motor component being a single button press in response to a circular trajectory once per block of eight trials. Since the activity in dorsal stream regions clearly differed depending on whether trajectories were low or high frequency and button presses did not differ between conditions, it is unlikely that activity in these regions was evoked by the limited motor output required in each block. Therefore, the activity we observed in dorsal stream regions strongly suggests that RF motion stimuli evoke activity in the mirror neuron system.

Our findings of greater BOLD signal and higher SVM weights in premotor and IPL regions in association with identifiable RF trajectories could be analogous to findings from other studies in which the degree of activity within regions of the MNS positively correlates with the familiarity of the motor action being viewed by an observer (Calvo-Merino, Glaser, Grèzes, Passingham, & Haggard, 2005; Calvo-Merino, Grèzes, Glaser, Passingham, & Haggard, 2006). In other words, recognizable movements that are part of the observer's own motor repertoire more strongly activate MNS regions than unfamiliar actions. Thus, in the current study, although dorsal stream premotor-parietal areas are activated by RF motion in general, the stronger activation they display for shapes that the observer is able to behaviorally distinguish might reflect the level at which the motor system "understands" a particular RF trajectory and also the observer's conscious ability to identify the shape. In future studies, it will be interesting to examine whether extensive training on the high-frequency RF shape discrimination might result in greater decoding of these shapes and higher activation in the frontal-parietal cortices.

Identification of RF static image shapes

For the RF static data, a conjunction analysis of regions demonstrating activity in both the low- and high-frequency shape conditions revealed activity in Brodmann Areas 17 and 18 of the occipital cortex, the medial PPC (precuneus region), and the premotor cortex (Figure 6c, Table 5). However, when the results of contrasting activity associated with low- and high-frequency static images is examined, no significant differences in premotor activity are apparent but there is significantly greater activity bilaterally in the medial posterior parietal cortex extending laterally into the superior and inferior parietal lobules, and bilaterally in a region extending across parts of the middle occipital gyrus, lateral occipital cortex, and middle temporal gyrus (Figure 6d, Table 7).

The absence of significantly greater premotor activity in response to low-frequency static RF shapes is in contrast to the equivalent comparison in the motion data which shows that both dorsal and ventral premotor activity is significantly greater in the low-frequency motion trajectory condition. Similarly, the

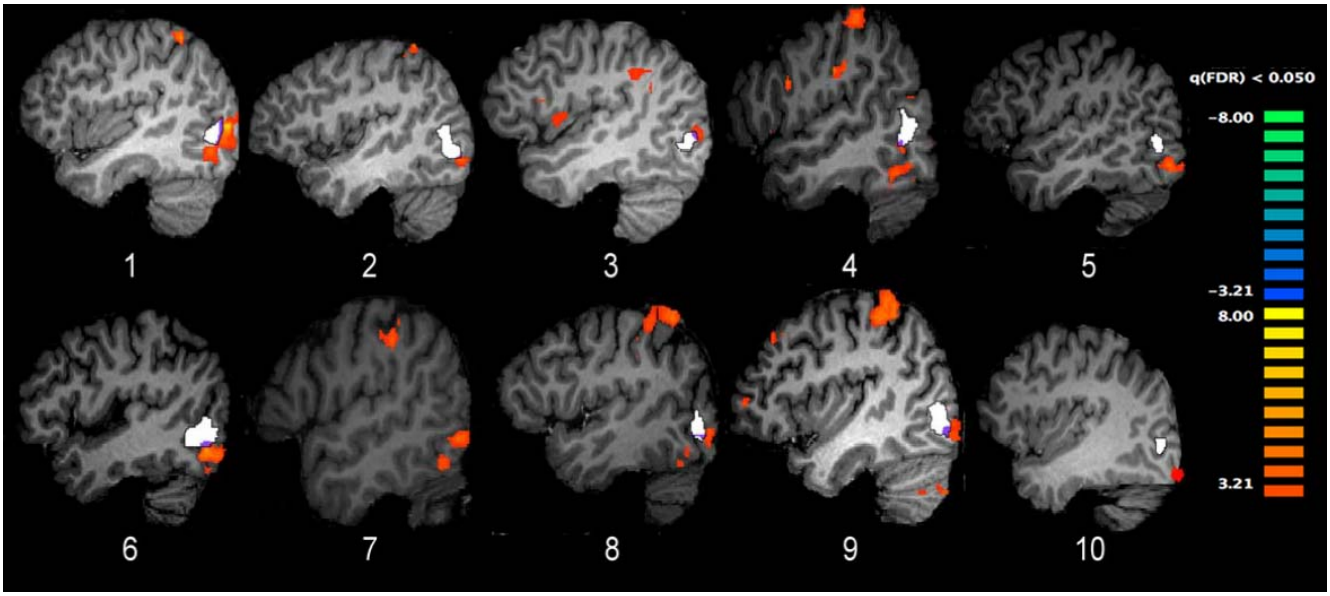

Figure 9. Results of a contrast between BOLD activity associated with low- versus high-frequency RF static image conditions in individual participants (false color overlays) relative to the location of individual MT regions defined by localizer scans (white overlays). MT was localized to a region that was generally slightly anterior-dorsal but adjacent to an occipital region that consistently demonstrated significantly greater activity in the low-frequency RF static condition. Most participants had a very small region of overlap between these two regions (shown in purple). Note that in Participant 7, MT was localized to a region slightly medial to occipital activity and could not be shown in the same slice as the contrast results.

whole-brain multivoxel analysis did not reveal any voxels with significantly higher SVM weights in the premotor region for comparisons of low- versus high-frequency shapes in the static image condition. Therefore, while the static stimuli clearly evoke some premotor activity, this activity likely does not play a role in shape recognition unless visual motion is present in the stimulus. However, the existence of premotor activity evoked by the static stimuli in general does raise a question. In particular, if the dorsal stream activity associated with the RF motion trajectories truly indicates that they are treated as potential motor actions, why would static versions of the stimuli activate similar cortical regions? Typically the mirror neuron system is much more active for moving stimuli than it is for static stimuli. Even so, others have observed that static photographs depicting human actions activate regions associated with the mirror neuron system (Proverbio, Riva, & Zani, 2009), suggesting that these regions can be activated by implied motion. Therefore, it is possible that in the current study, premotor activity in response to the static stimuli was a result of previous exposure to their motion trajectory equivalents which, aside from containing visual motion, were as similar as possible.

As stated above, the group contrast of activity evoked by low- versus high-frequency shapes also revealed significantly greater activity bilaterally at the intersections of the middle and lateral occipital regions and the middle temporal gyrus. To get a clearer idea of where this activity is localized in individual participants, we also examined this contrast separately in each observer using spatially unsmoothed data. The individual contrasts invariably demonstrated greater activity for the low-frequency static RF shapes in a region slightly posterior and ventral to the independently localized MT region (Figure 9). Anatomically, this region corresponds to the lateral occipital complex (Freeman, Sterzer, & Driver, 2012; Grill-Spector, Kourtzi, & Kanwisher, 2001; Larsson & Heeger, 2006). In the whole-brain group MVPA results, voxels in the LOC region also had significantly higher SVM weights for the low-frequency shapes, indicating a greater role in decoding frequency shapes. Unlike the high-frequency RF motion trajectories which were likely indistinguishable to observers, the behavioral data (see Figure 3) indicate that discrimination performance was above chance for the high-frequency static RF shapes, albeit variable across observers. Given the long exposure times (3 s), chosen to equate behavioral and fMRI conditions, it is possible that a different strategy such as counting "bumps" or cycles might have been at play for high-frequency shapes. Therefore, if one assumes that the low-frequency static images (which formed diamond- and star-like shapes) were more familiar and recognizable than the high-frequency static shapes, levels of activity in the LOC region may be associated with shape recognizability in a similar way that premotor and parietal activity appear to be for the RF motion trajectories. This idea is consistent with the increasingly well-known roles

of this ventral stream region in object recognition (see Grill-Spector, Kourtzi, & Kanwisher, 2001; Malach et al., 1995). Interestingly, a recent study examining object-selective processing in the LOC also used static RF shape stimuli (Silson et al., 2013). The findings presented by those authors demonstrate that LOC is likely subdivided into LO1 for processing of object orientation information and LO2 for processing of shape information. The Talairach coordinates described by the authors for LO2 match very well with the coordinates of voxels with significantly higher SVM weights associated with low-frequency static RF shapes in the current study, adding to our evidence that this region may indeed directly contribute to static RF shape processing and recognition.

Visual cue-invariant shape processing in the occipitotemporal and posterior parietal regions

A conjunction analysis of regions more active for low- versus high-frequency shapes in both the static and motion RF conditions revealed bilateral areas of activity in the occipitotemporal region and in the posterior parietal cortex (Figure 7, Table 8). It is possible that the potential perception of motion streaks in the RF motion trajectory stimuli could have contributed to regions of overlapping activity for the static and motion stimuli. If present, visible persistence effects may have resulted in perceptually static spatial cues that would be comparable in the moving and static RF stimuli, possibly contributing to some of the activity in common regions. However, it is likely that these regions of overlapping activity also resulted from visual cue-invariant shape processing. As discussed in the preceding section, within individual participants, contrasting BOLD activity related to low- versus high-frequency static RF shapes consistently revealed activity that was slightly posterior and ventral to independently localized MT regions (Figure 8). Interestingly, in most participants, there were small regions of overlap between these two areas even though the data were not spatially smoothed for these individual comparisons. This area of overlap generally corresponds well to the occipitotemporal region observed in the conjunction analysis for the RF motion and static data. This region was also more active for low- versus high-frequency shapes when RF motion data and static RF image data were analyzed separately. The commonality of this region to all of these analyses suggests that it could be involved in cue-invariant processing of shapes. Others have also observed considerable overlap of activity in this region evoked by static shapes defined by luminance or texture and that evoked by shapes that were defined by motion (Denys et al., 2004; Grill-Spector et al., 1998). Further examination of the nature of activity within this region, preferably with independent localizers for both MT and LOC will be needed to disentangle this region's specific roles in RF shape perception.

Along with the occipitotemporal region activity discussed in the preceding paragraph, the conjunction analysis for regions common to the motion and static stimuli also revealed activity in bilateral regions of the posterior parietal cortex. As with the occipitotemporal region, low-frequency shapes evoked greater activity than high-frequency shapes regardless of whether RF shapes were static or defined by motion. Thus, regions of the PPC are also potentially involved in cue-invariant RF shape processing.

In addition to these findings within the PPC from comparisons of BOLD signal amplitude, whole-brain multivoxel analyses revealed that within the PPC, regions of the inferior parietal lobule (IPL) are significantly more important for decoding the likely more recognizable low-frequency shapes than the less discriminable high-frequency shapes whether the cue contains motion or not (though the voxels do not overlap perfectly for the two conditions). The whole-brain multivoxel analysis did not localize voxels with these properties in the occipitotemporal region. Thus, while both the occipitotemporal and PPC regions localized with the between condition conjunction analysis are likely both involved in cue-invariant RF shape processing, the significant RFE results in the parietal cortex suggest that this region may be specifically involved in cue-invariant, conscious recognition of RF shapes.

The PPC is most often thought of as a dorsal stream region crucial to motor control. However, a role in shape processing in the PPC is not incongruent with the needs of the motor system. In order to interact with an object, the motor system must plan movements in the context of that object's physical characteristics, making access to shape information a necessity. In addition, our findings of a potentially cue-invariant shape processing PPC region are consistent with those of others who demonstrated the existence of lateral intraparietal (LIP) neurons with a definite role in eye movement preparation that also show object shape-dependent firing patterns which can occur in the absence of motor preparation (Sereno & Maunsell, 1998). These responses in the primate LIP are modulated by attention (Sereno & Amador, 2006) and a small subpopulation of neurons in this region display size and position invariance (Janssen, Srivastava, Ombelet, & Orban, 2008). Also, similar to the findings reported here, Murray, Olshausen, and Woods (2003) observed an area in humans that they refer to as the "parietal shape area" which spatially overlaps with the parietal activity we observed with our motion and static conjunction and RFE analyses. Consistent with our observations in the PPC, Murray et al. reported activity in this region that was associated with shape from both motion stimuli and static line drawings.

General conclusions

Comparisons of brain activity associated with RF motion trajectories and static RF images revealed that cue-invariant processing of these shapes occurs in the occipitotemporal and posterior parietal cortices. Further, the results of whole-brain multivoxel analysis combined with GLM contrast results suggest that this cue-invariance in the PPC is linked to global shape processing and/or the observer's conscious identification of an RF shape. In addition to these regions, the data presented here suggest that processing of RF shape also relies on visual cue-specific brain activity that depends on whether the RF shapes are defined by contrast or motion. In the case of the contrast-defined static RF shapes, conscious recognition of a given shape may require processing in the LOC region. In contrast, conscious recognition of RF shapes defined by motion trajectories likely includes processing in the premotor cortex.

Region of interest multivoxel results show that spatial patterns of voxel activity within visual regions V2, V3, and MT are capable of decoding RF motion trajectory shape regardless of whether the observer can consciously identify the shape or not. Thus, activity in these regions may be concerned with processing local properties rather than directly providing our conscious percept of global RF trajectory shape.

Our finding that RF motion trajectories activate regions associated with the dorsal stream mirror neuron system suggests that the brain processes these stimuli as motor possibilities rather than simply as purely visual experiences. It is possible that RF trajectories are seen as potential motor actions in themselves. For example, they could be visualized as a path that could be drawn or part of a nonverbal hand gesture. Or, they could be viewed as potential components of more complex movements such as the periodic trajectories observed at individual joints during repetitive motions like walking or riding a bicycle (Johansson, 1973; Johansson, 1976).

Keywords: radial frequency, fMRI, visual motion perception, dorsal visual stream, visual cue invariance

Acknowledgments

This work was supported by NSERC Discovery Grants #227224 to HRW and #007551 to FW.

Commercial relationships: none.
Corresponding author: Diana J. Gorbet.
Email: dgorbet@alumni.yorku.ca.
Address: Centre for Vision Research, York University, Toronto, ON, Canada.

References

Battaglia-Mayer, A., Caminiti, R., Lacquaniti, F., & Zago, M. (2003). Multiple levels of representation of reaching in the parieto-frontal network. *Cerebral Cortex, 13,* 1009–1022.

Calvo-Merino, B., Glaser, D. E., Grèzes, J., Passingham, R. E., & Haggard, P. (2005). Action observation and acquired motor skills: An fMRI study with expert dancers. *Cerebral Cortex, 15,* 1243–1249.

Calvo-Merino, B., Grèzes, J., Glaser, D. E., Passingham, R. E., & Haggard, P. (2006). Seeing or doing? Influence of visual and motor familiarity in action observation. *Current Biology, 16,* 1905–1910.

De Martino, F., Valente, G., Staeren, N., Ashburner, J., Goebel, R., & Formisano, E. (2008). Combining multivariate voxel selection and support vector machines for mapping and classification of fMRI spatial patterns. *NeuroImage, 43,* 44–58.

Denys, K., Vanduffel, W., Fize, D., Nelissen, K., Peuskens, H., Van Essen, D., … Orban, G. A. (2004). The processing on visual shape in the cerebral cortex of human and nonhuman primates: A functional magnetic resonance imaging study. *The Journal of Neuroscience, 24*(10), 2551–2565.

Engel, S. A., Glover, G. H., & Wandell, B. A. (1997). Retinotopic organization in human visual cortex and the spatial precision of functional MRI. *Cerebral Cortex, 7,* 181–192.

Freeman, E. D., Sterzer, P., & Driver, J. (2012). fMRI correlates of subjective reversals in ambiguous structure-from-motion. *Journal of Vision, 12*(6):35, 1–19, http://www.journalofvision.org/content/12/6/35, doi:10.1167/12.6.35. [PubMed] [Article]

Geisler, W. S. (1999). Motion streaks provide a spatial code for motion direction. *Nature, 400,* 65–69.

Gorbet, D. J., Wilkinson, F., & Wilson, H. R. (2012). An fMRI examination of the neural processing of periodic motion trajectories. *Journal of Vision, 12*(11):5, 1–15, http://www.journalofvision.org/content/12/11/5, doi:10.1167/12.11.5. [PubMed] [Article]

Grill-Spector, K., Kourtzi, Z., & Kanwisher, N. (2001). The lateral occipital complex and its role in object recognition. *Vision Research, 41,* 1409–1422.

Grill-Spector, K., Kushnir, T., Edelman, S., Itzchak, Y., & Malach, R. (1998). Cue-invariant activation

in object-related areas of the human occipital lobe. *Neuron, 21,* 191–202.

Grossman, E., Donnelly, M., Price, R., Pickens, D., Morgan, V., Neighbor, G., ... Blake, R. (2000). Brain areas involved in perception of biological motion. *Journal of Cognitive Neuroscience, 12,* 711–720.

Grossman, E. D., & Blake, R. (2001). Brain activity evoked by inverted and imagined biological motion. *Vision Research, 41,* 1475–1482.

Guyon, I., Weston, J., & Barnhill, S. (2002). Gene selection for cancer classification using support vector machines. *Machine Learning, 46,* 389–422.

Janssen, P., Srivastava, S., Ombelet, S., & Orban, G. A. (2008). Coding of shape and position in macaque lateral intraparietal area. *The Journal of Neuroscience, 28,* 6679–6690.

Johansson, G. (1973). Visual-perception of biological motion and a model for its analysis. *Perception & Psychophysics, 14,* 201–211.

Johansson, G. (1976). Spatio-temporal differentiation and integration in visual motion perception. An experimental and theoretical analysis of calculus-like functions in visual data processing. *Psychological Research, 38,* 379–393.

Ladewig, S. H. (2011). Putting the cyclic gesture on a cognitive basis. *CogniTextes, 6,* 1–25.

Larsson, J., & Heeger, D. J. (2006). Two retinotopic visual areas in human lateral occipital cortex. *The Journal of Neuroscience, 26,* 13128–13142.

Malach, R., Reppas, J. B., Benson, R. R., Kwong, K. K., Jiang, H., Kennedy, W. A., Ledden, P. J., Brady, T. J., Rosen, B. R., & Tootell, R. B. H. (1995). Object-related activity revealed by functional magnetic resonance imaging in human occipital cortex. *Proceedings of the National Academy of Sciences, USA, 92,* 8135–8139.

Murray, S. O., Olshausen, B. A., & Woods, D. L. (2003). Processing shape, motion and three-dimensional shape-from-motion in the human cortex. *Cerebral Cortex, 13,* 508–516.

Nichols, T. E., & Holmes, A. P. (2001). Nonparametric permutation tests for functional neuroimaging: A primer with examples. *Human Brain Mapping, 15,* 1–25.

Or, C. C.-F., Thabet, M., Wilkinson, F., & Wilson, H. R. (2011). Discrimination and identification of periodic trajectories. *Journal of Vision, 11*(8):7, 1–11, http://www.journalofvision.org/content/11/8/7, doi:10.1167/11.8.7. [PubMed] [Article]

Pasupathy, A. (2006). Neural basis of shape representation in the primate brain. *Progress in Brain Research, 154,* 293–313.

Peelen, M. V., & Wiggett, A. J. (2006). Patterns of fMRI activity dissociate overlapping functional brain areas that respond to biological motion. *Neuron, 49,* 815–822.

Proverbio, A. M., Riva, F., & Zani, A. (2009). Observation of static pictures of dynamic actions enhances the activity of movement-related brain areas. *PLoS One, 4*(5), 1–8.

Rizzolatti, G., & Matelli, M. (2003). Two different streams form the dorsal visual system: Anatomy and functions. *Experimental Brain Research, 153,* 146–157.

Rizzolatti, G., & Sinigaglia, C. (2010). The functional role of the parieto-frontal mirror circuit: Interpretations and misinterpretations. *Nature Reviews Neuroscience, 11,* 264–274.

Sereno, A. B., & Amador, S. C. (2006). Attention and memory-related response of neurons in the lateral intraparietal area during spatial and shape-delayed match-to-sample tasks. *The Journal of Neurophysiology, 95,* 1078–1098.

Sereno, A. B., & Maunsell, J. H. R. (1998). Shape selectivity in primate lateral intraparietal cortex. *Nature, 395,* 500–503.

Sereno, M. I., Dale, A. M., Reppas, J. B., Kwong, K. K., Belliveau, J. W., Brady, T. J., Rosen, B. R., & Tootell, R. B. (1995). Borders of multiple visual areas in humans revealed by functional magnetic resonance imaging. *Science, 268,* 889–893.

Silson, E. H., McKeefry, D. J., Rodgers, J., Gouws, A. D., Hymers, M., & Morland, A. B. (2013). Specialized and independent processing of orientation and shape in visual field maps LO1 and LO2. *Nature Neuroscience, 16,* 267–269.

Slotnick, S. D., & Yantis, S. (2003). Efficient acquisition of human retinotopic maps. *Human Brain Mapping, 18,* 22–29.

Tsai, P.-S., Shah, M., Keiter, K., & Kasparis, T. (1994). Cyclic motion detection for motion based recognition. *Pattern Recognition, 27,* 1591–1603.

Wilkinson, F., Wilson, H. R., & Haback, C. (1998). Detection and recognition of radial frequency patterns. *Vision Research, 38,* 3555–3568.

Xiong, Y., & Quek, F. (2006). Hand motion gesture frequency properties and multimodal discourse analysis. *International Journal of Computer Vision, 69,* 353–371.